11

A simulated annealing band selection approach for high-dimensional remote sensing images

Yang-Lang Chang and Jyh-Perng Fang
Department of Electrical Engineering National Taipei University of Technology,Taipei Taiwan

1. Introduction

State-of-the-art sensors can make use of a growing number of spectral bands. Data initially developed in a few multispectral bands today can be collected from several hundred hyperspectral and even thousands of ultraspectral bands. This recent technology finds application in many domains, including satellite based geospatial technology, monitoring systems, medical imaging, and industrial product inspection. High-dimensional images provide large spectral information for subsequent data analysis. While images are continuously being acquired and archived, existing methods have proved inadequate for analyzing such large volumes of data. As a result, a vital demand exists for new concepts and techniques for treating high-dimensional datasets.

A common issue in hyperspectral image classification is how to improve class separability without incurring the curse of dimensionality Bellman (1961). This problem has occupied various research communities, including statistics, pattern recognition, and data mining. Researchers all describe the difficulties associated with the feasibility of distribution estimation. Accordingly, selecting the most valuable and meaningful information has become ever more important. Numerous techniques were developed for *feature extraction* and *band selection* to reduce dimensionality without loss of class separability for dealing with high-dimensional datasets Bruce et al. (2002); Jimenez & Landgrebe (1999); Jimenez-Rodriguez et al. (2007); Plaza et al. (2005); Tu et al. (1998); Wang & Chang (2006). The most widely used approach is the *principal components analysis* (PCA) which reorganizes the data coordinates in accordance with data variances so that features are extracted based on the magnitudes of their corresponding eigenvalues Richards & Jia (1999). Further *Fisher discriminant analysis* uses the between-class and within-class variances to extract desired features and reduce dimensionality Duda & Hart (1973). They focus on the estimation of statistics at full dimensionality to extract classification features. For example, conventional PCA assumes the covariances of different classes are the same. It treats the data as if it is a single distribution of different classes. The potential differences between class covariances are not explored.

In our previous work, a *greedy modular eigenspace* (GME) Chang, Han, Fan, Chen, Chen & Chang (2003) approach was proposed to solve this problem. The GME *band selection* (GMEBS)

was developed by clustering highly correlated bands into a smaller subset based on the *greedy algorithm* and was proved to be a fast and effective method for *supervised-band-subset selection* (also named *feature selection*). It divides the data into different classes and overcomes the dependency on global statistics, while preserving the inherent separability of different classes. Most classifiers seek only one set of features that discriminates all classes simultaneously. This not only requires a large number of features, but also increases the complexity of the potential decision boundary. GMEBS method solves this problem and speeds up the feature extraction processes significantly. Although GMEBS can provide acceptable results for *feature selection* and *dimensionality reduction*, it consumes a large amount of computation to obtain a solution by a *greedy algorithm*. Unfortunately, it is also hard to find the optimal (maximum) or near-optimal (near-maximum) set by *greedy algorithm* except by exhaustive iteration. The long execution time of this exhaustive iteration has been the major drawback in practice. Accordingly, finding the optimal or near-optimal solution is very expensive.

Correspondingly, finding an efficient alternative has become necessary to overcome the above mentioned drawback of GMEBS. One consequence is the development of a technique known as *simulated annealing* (SA) Greene & Supowit (1984); Kirkpatrick et al. (1983) for feature extraction of high- dimensional datasets. Instead of adopting the band-subset-selection paradigm underlying the *greedy optimization* approach of GMEBS, we introduce *simulated annealing band selection* (SABS), which makes use of the *heuristic optimization algorithm* to collect the subsets of non-correlated bands for hyperspectral images to overcome this disadvantage. SA optimization has been widely adopted in fields such as electronics design automation Fang et al. (2004; 2006). The proposed SABS can readily select each band and sort different classes into the most common band subset. It can not only speed up the procedure to simultaneously select the most significant features according to the SA *optimization scheme*, but also make use of the hyperspatial characteristics embedded in GME features.

The performance of the proposed SABS is evaluated by fusing *MODIS/ASTER airborne simulator* (MASTER), a hyperspectral sensor, and airborne *synthetic aperture radar* (SAR) images for land cover classification during the Pacrim II campaign. Experimental results demonstrated that the proposed SABS approach is an effective method for dimensionality reduction and feature extraction. Compared to GMEBS, SABS can not only effectively group highly correlated bands, but also consume less resources. This chapter is organized as follows. In Section 2, the proposed SABS is described in detail. In Section 3, a set of experiments is conducted to demonstrate the feasibility and utility of the proposed SABS approach. Finally, in Section 4, some conclusions are outlined.

2. Methodology

2.1 Review of GMEBS

A visual *correlation matrix pseudo-color map* (CMPM) which was proposed by Lee & Landgrebe (1993) is used in Fig. 1 to emphasize the second-order statistics in hyperspectral data and to illustrate the magnitude of correlation matrices in the GMEBS method. Also shown in Fig. 1 is GME set $\mathbf{\Phi}^k$, $\mathbf{\Phi}^k = (\Phi_1^k, \dots \Phi_l^k, \dots \Phi_{n_k}^k)$, for class $\mathbf{W}_k$, which we previously proposed Chang, Han, Fan, Chen, Chen & Chang (2003); Chang et al. (2004). It illustrates the original CMPM and the reordered one after GMEBS. Each modular eigenspace Φ_l^k, subset of GME, includes a subset of highly correlated bands. Each ground cover type or material class has a distinct set

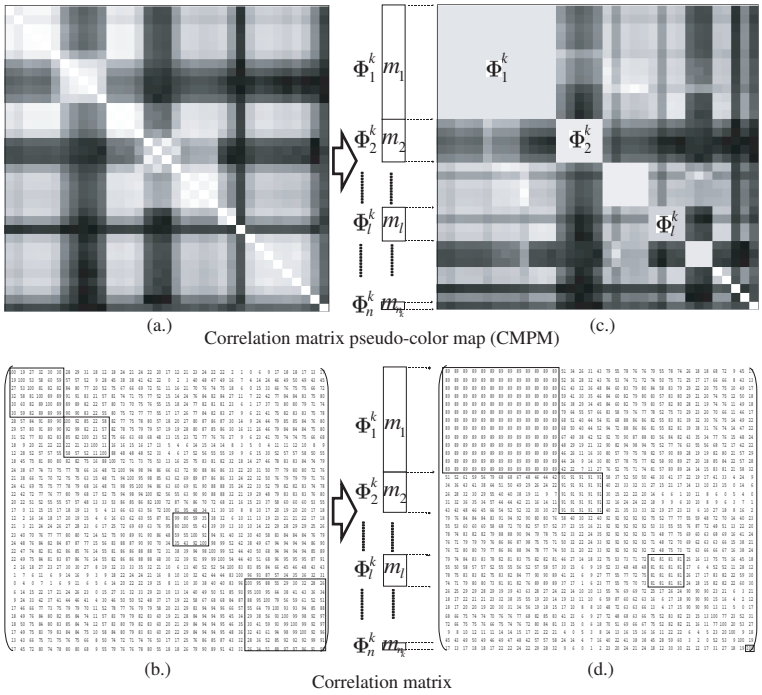

Fig. 1. An example illustrating (a) an original CMPM, (b) its corresponding correlation matrix for class k, (c) the GME set for class k, and (d) its corresponding correlation matrix after SA band selection.

of GME-generated *feature eigenspaces*.

GMEBS is a spectral-based technique that explores the correlation among bands. It utilizes the inherent separability of different classes in high-dimensional data to reduce dimensionality and formulate a unique GME feature. GMEBS performs a *greedy* iteration searching algorithm which reorders the correlation coefficients in the data correlation matrix row by row and column by column simultaneously, and groups highly correlated bands as GME *feature eigenspaces* that can be further used for *feature extraction* and *selection*. Reordering the bands in terms of wavelengths in high-dimensional data sets, without regard for the original order, is an important characteristic of GMEBS. Fig. 2 shows the graphical mechanism of GMEBS spectral band reordering. After finding GME sets $\mathbf{\Phi}^k$ for all classes $\mathbf{W}_k$, $k \in \{1, \ldots, N\}$, a fast and effective *feature scale uniformity transformation* (FSUT) Chang, Chen, Han, Fan, Chen & Chang (2003); Chang et al. (2004) is performed to unify the feature scales of these GME sets into an *identical* GME (IGME) set $\mathbf{\Phi}_I$. It uses *intersection* (AND) operations applied to the band numbers inside each GME module $\mathbf{W}_k$ to unify the feature scales of different classes. The concept block diagram of GMEBS is shown in Fig. 3 (a). Every different class has the same IGME set $\mathbf{\Phi}_I$ after GMEBS.

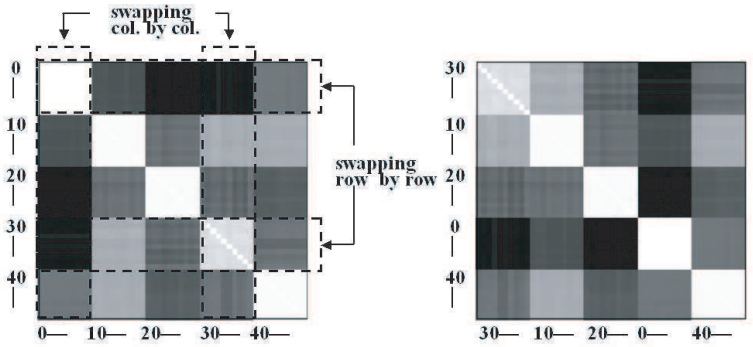

Fig. 2. The original CMPM (White=1 or -1; black=0) and the CMPM after reordering band Nos.0-9 and 30-39.

GMEBS defines a correlation submatrix $\mathbf{c}_{\Phi_l^k}[m_l][m_l]$ which belongs to the l^{th} modular eigenspace (Φ_l^k) of GME $\mathbf{\Phi}^k$, $\mathbf{\Phi}^k = (\Phi_1^k, \ldots \Phi_l^k, \ldots \Phi_{n_k}^k)$, for a land cover class $\mathbf{W}_k$ in the dataset, where m_l and n_k respectively represent the number of bands (features) in the modular eigenspace Φ_l^k, and the total number of modular eigenspaces in the GME set $\mathbf{\Phi}^k$, i.e. $l \in \{1, \ldots, n_k\}$, as shown in Fig. 1. The original correlation matrix $\mathbf{c}_{X^k}[m_t][m_t]$, where m_t is the total number of original bands (i.e. $m_t = \sum_{l=1}^{n_k} m_l$), is decomposed into n_k correlation submatrices $\mathbf{c}_{\Phi_1^k}[m_1][m_1], \ldots \mathbf{c}_{\Phi_l^k}[m_l][m_l], \ldots \mathbf{c}_{\Phi_{n_k}^k}[m_{n_k}][m_{n_k}]$ to build the GME set $\mathbf{\Phi}^k$ for the class $\mathbf{W}_k$. There are $\frac{m_t!}{2}$ (a half factorial of m_t) possible combinations to construct a GME candidate $\mathbf{\Phi}^k$. It is computationally expensive to make an exhaustive search to find the optimal GME set $\mathbf{\Phi}^k$ if m_t is a large number. In order to find the near-optimal GME set $\mathbf{\Phi}^k$ of class $\mathbf{W}_k$, a *heuristic optimization algorithm* of SA-based band reordering algorithm is therefore applied to SABS method.

2.2 SABS

A common technique in metallurgy, SA denotes the slow-cooling melt behavior in the formation of hardened metals. Two decades ago scientists recognized the similarities between a simulated annealing process and a best-solution search for a combinatorial optimization problem Kirkpatrick et al. (1983). SA provides an *annealing schedule* that starts at an effective high temperature and gradually decreases until it is slightly above zero. The *heuristic optimization algorithm* is performed in a nested loop fashion at various designated temperatures. Advantages of SA include escape from local minima at non-zero temperatures, early appearance of gross features of final state at highest temperatures, and emergence of some finer details at lower temperatures.

SABS collects GME sets $\mathbf{\Phi}^k$ from high-dimensional images of different classes simultaneously based on the *simulated annealing optimization algorithm*. Each modular eigenspace Φ_l^k includes a subset of highly correlated bands. SABS scheme has a number of merits. 1.) GMEBS tends to collect the bands into a subset with highly correlated covariance to avoid a potential bias

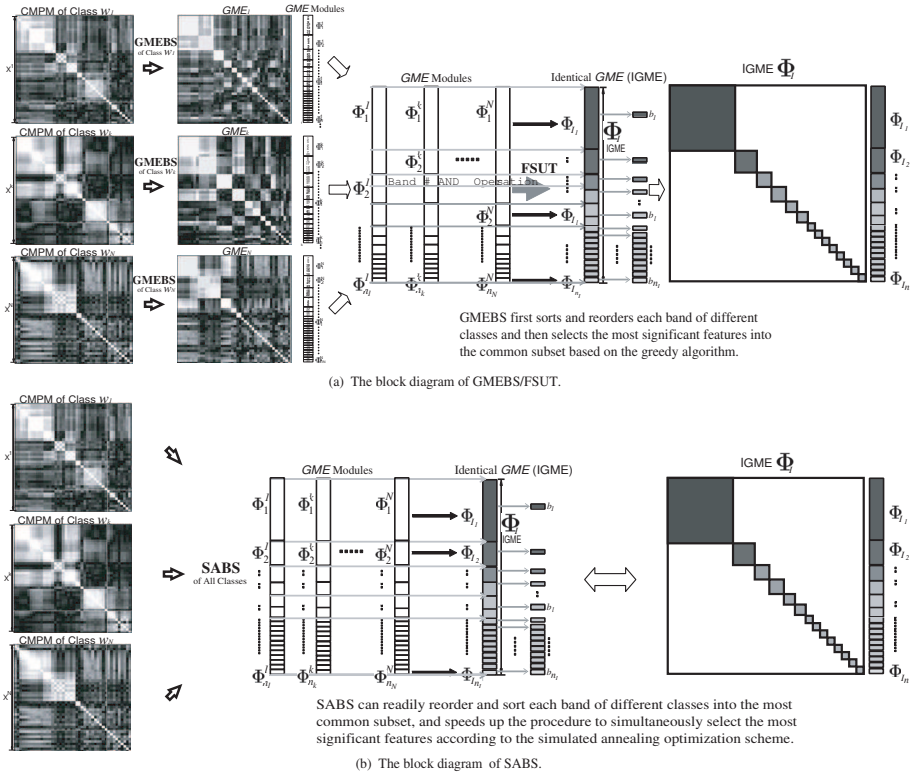

Fig. 3. An illustration of the differences between (a) FSUT/GMEBS and (b) the proposed SABS methods.

problem that may occur in PCA Jia & Richards (1999). 2.) Unlike traditional PCA, it avoids the bias problems that arise from transforming the information into linear combinations of bands. 3.) In addition, it can further extend the search and convergence abilities in the solution space based on *simulated annealing method* to reach the global optimal or near-optimal solution and escape from local minima. 4.) Finally, it takes advantage of the special characteristics of GME to readily reorder and sort each band of different classes into the most common feature subspaces according to the SA *optimization scheme*.

For each class $\mathbf{W}_k$, $k \in \{1, \ldots, N\}$, SABS performs SA-based iterations to build an IGME set $\mathbf{\Phi}_I^k$. Unlike GMEBS that first sorts and reorders each band of different classes based on the *greedy* algorithm and then selects the significant features IGME set $\mathbf{\Phi}_I^k$ by FSUT Chang, Chen, Han, Fan, Chen & Chang (2003); Chang et al. (2004), the proposed SABS can readily reorder and sort each band of different classes into the most common subset, and speeds up the procedure to simultaneously select IGME set $\mathbf{\Phi}_I^k$ based on SA *optimization scheme*. An illustration of the differences between GMEBS/FSUT and SABS methods is shown in Fig. 3. SABS collects the same band numbers located in each modular eigenspace Φ_I^k of all different classes

$\mathbf{W}_k$ ($k \in \{1, \ldots, N\}$) simultaneously.

The proposed SABS scheme is as follows:

1) Perturbation: SABS optimization algorithm is performed in two nested loops. They are Markov chains and temperature reduction cycles. After initialization, the cost can be produced by the permutation as shown in Fig. 4. Two bands associated with correlation matrix $\mathbf{c}_{X^k}[m_t][m_t]$ are randomly swapped (switched) for all classes, $\mathbf{W}_k$, $k \in \{1, \ldots, N\}$, where m_t is the total number of original bands for all of different classes $\mathbf{W}_k$, $k \in \{1, \ldots, N\}$, at the same time.

2) Cost function: After each perturbation, the cost is obtained by accumulating the *values of correlation coefficient* $VCC_{\Phi_l^k}[i][j]$ for the corresponding correlation submatrices $\mathbf{c}_{\Phi_1^k}[m_1][m_1]$, $\ldots \mathbf{c}_{\Phi_l^k}[m_l][m_l], \ldots \mathbf{c}_{\Phi_{n_k}^k}[m_{n_k}][m_{n_k}]$ of modular eigenspaces Φ_l^k, $i, j \in \{1, \ldots, m_l\}$, $l \in \{1, \ldots, n_k\}$ and $k \in \{1, \ldots, N\}$, as shown in Eq. 1,

$$cost = \frac{1}{\sum_{k=1}^{N} \sum_{l=1}^{n_k} \sum_{i=1}^{m_l} \sum_{j=1}^{m_l} |VCC_{\Phi_l^k}[i][j]|}, \tag{1}$$

where m_l and n_k represent the number of bands (feature spaces) in modular eigenspaces Φ_l^k, and the total number of modular eigenspaces of GME set Φ^k, $l \in \{1, \ldots, n_k\}$, respectively. $VCC_{\Phi_l^k}[i][j]$ is located at the i^{th} row and the j^{th} column of the l^{th} correlation submatrix $\mathbf{c}_{\Phi_l^k}[m_l][m_l]$ for all of the class $\mathbf{W}_k$, $k \in \{1, \ldots, N\}$.

3) Annealing schedule: At the initial temperature T_0, the annealing starts with the original correlation matrix $\mathbf{c}_{X^k}[m_t][m_t]$ for all of the class $\mathbf{W}_k$, $k \in \{1, \ldots, N\}$. The temperature decreases steadily, $T_x = r^x T_0$, where $r = 0.85$ and $x = 1, 2, 3, \cdots$. Band-swapping is performed at each temperature K, where $5 \leq K \leq 10$. The *annealing process* terminates when number of accepted swapping is smaller (< 0.05) or temperature is low enough.

The operations of proposed SA band swapping algorithm is shown in Fig. 4, wherein P, ε, r, K are parameters for tuning the SA band swapping algorithm. T_0, reported in Line 2, is an initial temperature and Δavg is an average of cost change after a sequence of random band swapping. Parameter P is chosen such that $P = e^{-\Delta avg/T_0} \approx 1$ and consequently enables a higher probability of accepting *uphill* at high temperatures. The rest of the parameters are given empirically. Parameter ε is the terminated temperature, r is the decreasing rate of temperature, and K is used to control the counts of perturbation at each temperature. The *Markov chain MT* is determined by parameter K and the problem size N. The variables *uphill*, and *reject* are used to control the numbers of perturbation at each temperature. In addition, both variables are used to observe the performance of proposed SABS and consequently to help constructing an effective *annealing schedule*.

In the pseudo code, *Random* shown in Line 8 is a floating number generated from a random function, which ranges between 0 and 1. The probabilities of going *uphill* (paying higher costs) decrease as temperatures fall in *the annealing schedule*, which is controlled by the Boltzmann factor $e^{-\Delta cost/T}$. At each temperature, the band swappings (perturbations) are repeated until either there are n downhill perturbations or the total number of perturbations exceeds 2n

SA_Band_Swapping Algorithm (P, ε, r,K)

```
1  CM ← original correlation matrix;
2  Best ← CM;  T ← Δavg / log(P); MT← uphill ← 0;  n ←KN;
3  repeat - // Temperature reduction cycles
4    MT ← uphill ← reject ← 0;
5    repeat - // Markov chains
6       New_CM ← band_swapping(CM);
7       MT← MT + 1;  Δcost ← cost(New_CM) - cost(CM);
8       if (Δcost ≤ 0) or (Random < e^(-Δcost/T)) then
9          if (Δcost > 0) then uphill ← uphill + 1;
10         CM ← New_CM;
11         if cost(CM) < cost(Best) then Best←CM;
12      else reject ← reject + 1;
13    until (uphill > n ) or (MT > 2 n);
14    T ← rT;
15 until (reject / MT > 0.95) or (T < ε);
```

Fig. 4. SA band swapping algorithm.

where n is the number of spectral bands. The annealing process is terminated either when the number of accepted perturbations is less than 5% of all perturbations occurring at a certain temperature or when the temperature is low enough.

The basic components for the SA algorithm include solution space, neighborhood structure, cost function, and annealing schedule. To solve an optimization problem using SA, proper arrangement of these components is necessary. The solution space is defined by all possible combinations of swapping rows and columns in the original CMPM spaces. The modular eigenspace Φ_l^k is constructed by randomly swapping two bands among the associated correlation matrices of different classes. SABS makes use of the SA cost function to constrain the values of *correlation coefficients VCCs* within a threshold range of 0.70 to 0.92. The cost function is obtained by accumulating the *VCCs* inside the modular eigenspaces Φ_l^k of different classes.

Eventually, an IGME set $\mathbf{\Phi}_I$ is composed. For convenience, we sort these IGME feature modules Φ_{I_l}, where $l \in \{1, \ldots, n_I\}$, according to the number of their feature bands, i.e. the number of feature spaces in descending order. Each IGME feature module Φ_{I_l} has a unique band set inside a modular eigenspace Φ_l^k box as illustrated in Fig. 3. Compared to the GMEBS/FSUT, the proposed SABS can not only speed up the computation by taking into account the IGME feature module Φ_{I_l} of different classes at the same time, but also improve the features extracted from the most common GME $\mathbf{\Phi}^k$ of different classes simultaneously. Furthermore, SABS provides a quick procedure for band selection to find the most significant hyperspectral features compared to GMEBS and the other conventional feature extraction methods.

Fig. 5. The map of the Au-Ku test site used in the experiment.

3. Experimental Results

A plantation area in Au-Ku on the east coast of Taiwan as shown in Fig. 5 was chosen for investigation. The image data was obtained by the MASTER and SAR instrument as part of the PacRim II project Hook et al. (2000). A ground survey was made of the selected six land cover types at the same time. The proposed SABS was applied to 35 bands selected from the 50 contiguous bands (excluding the low signal-to-noise ratio mid-infrared channels) of MASTER Hook et al. (2000) and nine components of AIRSAR. Nine components in the polarimetric SAR covariance matrix are preprocessed Lee et al. (1999). Six land cover classes, sugar cane A, sugar cane B, seawater, pond, bare soil and rice ($N = 6$) are used in the experiment. The *k-nearest neighbor* (KNN) classifier was used to test the effectiveness of SABS. The criterion for calculating the classification accuracy of experiments was based on exhaustive test cases. One hundred and fifty labeled samples were randomly collected from ground survey datasets by iterating every fifth sample interval for each class. Thirty labeled samples were chosen as training samples, while the rest were used as test samples, i.e. the samples were partitioned into 30 (20%) training and 120 (80%) test samples ($M = 120$) for each test case. Eighteen correlation coefficient thresholds, $VCCs = 0.70 \sim 0.92$ with a offset of 0.01, were selected to carry out the experiments.

The parameters used for SABS are initialized as follows. The probability to accept higher cost is decreased following the decreased temperature, and the decreasing rate of temperature is 0.95, the terminating temperature is 100 Celsius degree (^oC), while the factor deciding the number of perturbation at a specified temperature is 20. We examined the effectiveness and robustness of the SABS with initial temperatures differentiating from 100,000Ű900,000 degrees Celsius. Finally, all of the multiple combinations of parameters stated above are averaged to obtain the experimental results. Table 1 summarizes the evaluation of classification accuracy under a different initial temperature to illustrate the validity of these unique properties of

	offset (%)				
Initial temperature	50	60	70	80	90
10000	99.67%	91.28%	100.00%	90.84%	100.00%
30000	93.31%	100.00%	99.84%	91.00%	94.68%
50000	100.00%	92.93%	100.00%	92.38%	99.89%
70000	100.00%	100.00%	89.80%	92.38%	99.78%
90000	95.45%	99.40%	89.42%	100.00%	91.01%

Table 1. Summary evaluation of classification accuracy for SABS scheme.

proposed SABS method. These encouraging results showed that satisfactory classification accuracy could be achieved with only a few computational time and small training samples.

Interestingly, two comparisons of both *dimensionality reduction rate* (DRR) and *variance of classification accuracy* (VCA) according to different *VCCs* are also illustrated. The DRR and VCA are used to validate the performances of the proposed SABS as shown defined in Eq. 2 and Eq. 4 respectively.

$$DRR = \frac{m_t - n_k}{m_t} \times 100\%, \tag{2}$$

where m_t and n_k represent the total number of original bands (i.e. $m_t = \sum_{l=1}^{n_k} m_l$), and the total number of modular eigenspaces in the GME set $\mathbf{\Phi}^k$ respectively Chang, Han, Fan, Chen, Chen & Chang (2003).

$$VCA = \frac{\sum_{i=1}^{n} (Acc_i - \mu_i)^2}{n}, \tag{3}$$

where n represents the number of times to arbitrarily choose three bands respectively from the three larger SABS modular eigenspace Φ_l^k for the classification operations. Acc_i is the corresponding classification accuracy of the above operations. The mean μ is equal to $\frac{\sum_{i=1}^{n} Acc_i}{n}$.

Fig. 6 summarizes the evaluation results that have the same *costs*, namely *quality of solutions*, to illustrate the validity of proposed SABS. The criteria for the SABS performance evaluations in Fig. 6 (a.) and (b.) are based on different experimental benchmarks with the same *quality of solution*. Furthermore, an evaluation of classification efficiency $(CE = \xi)$,

$$\xi = \frac{DRR}{VCA}, \tag{4}$$

as shown in Fig. 7, is also designed to validate the contributions of proposed SABS. The results appearing in Fig. 7 show that an *efficient critical point* around $VCC = 0.91$ can be reached to obtain a high DRR accompanied with a low VCA impact when SABS is applied to the high-dimensional datasets.

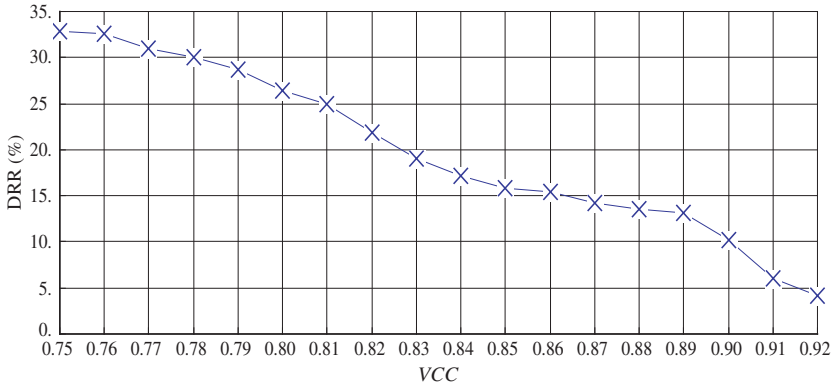

(a). SABS DRR comparison

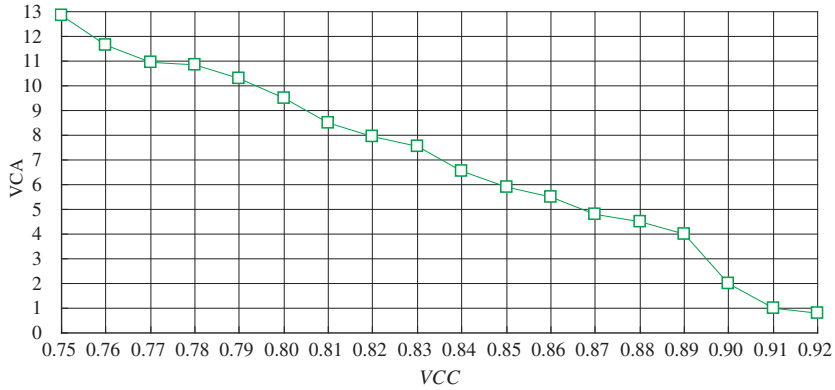

(b). SABS VCA comparison

Fig. 6. Two SABS performance comparisons of (a.) DRR and (b.) VCA with different thresholds of VCCs.

4. Conclusions

This chapter presents a novel SABS technique for *feature selection* and *dimensionality reduction* of hyperspectral and SAR images. Reordering the bands regardless of the original order in terms of wavelengths in high-dimensional datasets is an important characteristic of SABS. It is proposed to overcome the drawback of GMEBS which has a long execution time during the exhaustive iteration to obtain a solution by the *greedy algorithm*. By adopting the band-subset-selection paradigm underlying the *heuristic optimization algorithm*, the proposed SABS can not only readily find the most significant GME subsets, but also further extend the search abilities in the solution space to reach the global optimal or near-optimal solution and escape from local minima based on *simulated annealing method*.

Encouraging experimental results showed that the feature bands selected by SABS algorithm from high-dimensional remote sensing images contain robust discriminatory properties cru-

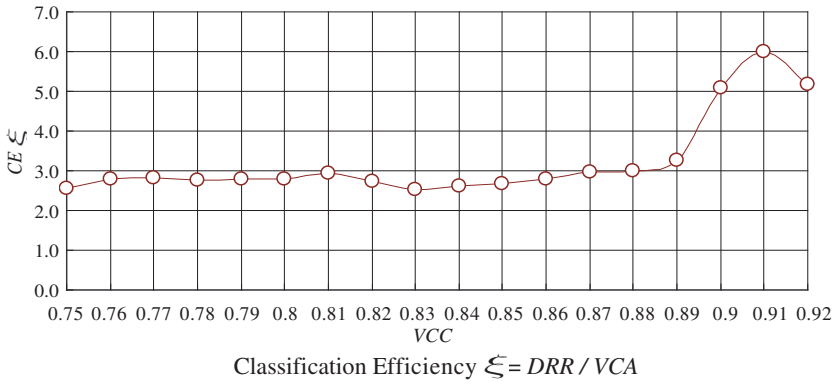

Fig. 7. The SABS classification efficiency comparison with different thresholds of VCCs.

cial to subsequent classification. They make use of the potential significant separability embedded in GME to select a unique set of most important feature bands in high-dimensional datasets. The experimental results also demonstrated that the proposed SABS can significantly improve the computational loads and provide a more reliable quality of solution compared to the GMEBS method. The proposed evaluation of $CE(\xi)$ provides an objective criterion to determine a suitable and appropriate value of VCC, and to obtain a high quality DRR accompanied with a lower VCA impact. Besides the subjects discussed in this chapter, how to find the best tradeoff among the global search, accuracy, and computational cost will be the issues of our future studies.

Acknowledgment

This work was supported by the National Science Council, Taiwan, under Grant Nos. NSC 98-2116-M-027-002 and NSC 99-2116-M-027-003, and Ministry of Economic Affairs, Taiwan, under Grant No. 98-EC-17-A-02-S2-0021.

5. References

Bellman, R. E. (1961). *Adaptive Control Processes: A Guided Tour*, Princeton University Press, New Jersey, NJ.

Bruce, L. M., Koger, C. H. & Li, J. (2002). Dimensionality reduction of hyperspectral data using discrete wavelet transform feature extraction, *IEEE Trans. Geosci. Remote Sensing* **40, Issue: 10**: 2331–2338.

Chang, Y. L., Chen, C. T., Han, C. C., Fan, K. C., Chen, K. S. & Chang, J. H. (2003). Hyperspectral and sar imagery data fusion with positive boolean function, Vol. 5093 of *Proc. SPIE*, pp. 765–776.

Chang, Y. L., Han, C. C., Fan, K. C., Chen, K. S., Chen, C. T. & Chang, J. H. (2003). Greedy modular eigenspaces and positive boolean function for supervised hyperspectral image classification, *Optical Engineering* **42, no. 9**: 2576–2587.

Chang, Y. L., Han, C. C., Ren, H., Chen, C.-T., Chen, K. S. & Fan, K. C. (2004). Data fusion of hyperspectral and sar images, *Optical Engineering* **43, no. 8**: 1787–1797.

Duda, R. & Hart, P. (1973). *Pattern Classification and Scene Analysis*, John Wiley & Sons, New York.

Fang, J. P., Tong, Y. S. & Chen, S. J. (2004). Simultaneous routing and buffering in floorplan design, Vol. 151, no. 1 of *IEE Proc. Computers and Digital Techniques*, pp. 17–22.

Fang, J. P., Tong, Y. S. & Chen, S. J. (2006). An enhanced bsa for floorplanning, *IEICE Trans. Fundamentals* **E89-A, no. 2**: 528–534.

Greene, J. & Supowit, K. (1984). Simulated annealing without rejected moves, Proc. Int'l Conf. on Computer Designs, pp. 658–663.

Hook, S. J., Myers, J. J., Thome, K. J., Fitzgerald, M. & Kahle, A. B. (2000). The modis/aster airborne simulator (master) - a new instrument for earth science studies, *Remote Sensing of Environment* **76, Issue 1**: 93–102.

Jia, X. & Richards, J. A. (1999). Segmented principal components transformation for efficient hyperspectral remote-sensing image display and classification, *IEEE Trans. Geosci. Remote Sensing* **37, no. 1**: 538–542.

Jimenez, L. O. & Landgrebe, D. A. (1999). Hyperspectral data analysis and supervised feature reduction via projection pursuit, *IEEE Trans. Geosci. Remote Sensing* **37, Issue: 6**: 2653–2667.

Jimenez-Rodriguez, L. O., Arzuaga-Cruz, E. & Velez-Reyes, M. (2007). Unsupervised linear feature-extraction methods and their effects in the classification of high-dimensional data, *IEEE Trans. Geosci. Remote Sensing* **45, Issue: 2**: 469–483.

Kirkpatrick, S., Gelatt, C. D. & Vecchi, M. P. (1983). Optimization by simulated annealing, *Science* **220, no. 4598**: 671–680.

Lee, C. & Landgrebe, D. A. (1993). Analyzing high-dimensional multispectral data, *IEEE Trans. Geosci. Remote Sensing* **31, no. 4**: 792–800.

Lee, J. S., Grunes, M. R., Ainsworth, T. L., Du, L. J., Schuler, D. L. & Cloude, S. R. (1999). Unsupervised classification using polarimetric decomposition and the complex wishart classifier, *IEEE Trans. Geosci. Remote Sensing* **37, no. 5**: 2249–2258.

Plaza, A., Martinez, P., Plaza, J. & Perez, R. (2005). Dimensionality reduction and classification of hyperspectral image data using sequences of extended morphological transformations, *IEEE Trans. Geosci. Remote Sensing* **43, Issue: 3**: 466–479.

Richards, J. A. & Jia, X. (1999). *Remote Sensing Digital Image Analysis, An Introduction, 3rd ed.*, Springer-Verlag, New York.

Tu, T.-M., Chen, C.-H., Wu, J.-L. & Chang, C.-I. (1998). A fast two-stage classification method for high-dimensional remote sensing data, *IEEE Trans. Geosci. Remote Sensing* **36, Issue: 1**: 182–191.

Wang, J. & Chang, C.-I. (2006). Independent component analysis-based dimensionality reduction with applications in hyperspectral image analysis, *IEEE Trans. Geosci. Remote Sensing* **44, Issue: 6**: 1586–1600.

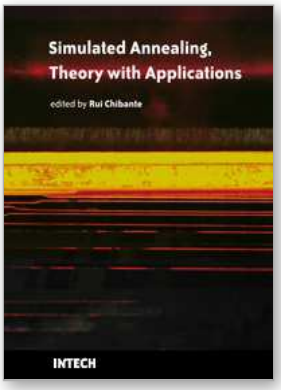

Simulated Annealing, Theory with Applications

Edited by Rui Chibante

ISBN 978-953-307-134-3
Hard cover, 292 pages
Publisher Sciyo
Published online 18, August, 2010
Published in print edition August, 2010

The book contains 15 chapters presenting recent contributions of top researchers working with Simulated Annealing (SA). Although it represents a small sample of the research activity on SA, the book will certainly serve as a valuable tool for researchers interested in getting involved in this multidisciplinary field. In fact, one of the salient features is that the book is highly multidisciplinary in terms of application areas since it assembles experts from the fields of Biology, Telecommunications, Geology, Electronics and Medicine.

InTech Europe
University Campus STeP Ri
Slavka Krautzeka 83/A
51000 Rijeka, Croatia
Phone: +385 (51) 770 447
Fax: +385 (51) 686 166
www.intechopen.com

InTech China
Unit 405, Office Block, Hotel Equatorial Shanghai
No.65, Yan An Road (West), Shanghai, 200040, China
中国上海市延安西路65号上海国际贵都大饭店办公楼405单元
Phone: +86-21-62489820
Fax: +86-21-62489821